Scripta Materialia 135 (2017) 54–58

Contents lists available at ScienceDirect

Scripta Materialia

journal homepage: www.elsevier.com/locate/scriptamat

Regular Article

Resistance of CoCrFeMnNi high-entropy alloy to gaseous hydrogen embrittlement

Yakai Zhao [a], Dong-Hyun Lee [a], Moo-Young Seok [a], Jung-A Lee [a], M.P. Phaniraj [b], Jin-Yoo Suh [b,*], Heon-Young Ha [c], Ju-Young Kim [d], Upadrasta Ramamurty [e], Jae-il Jang [a,*]

[a] Division of Materials Science and Engineering, Hanyang University, Seoul 04763, Republic of Korea
[b] High Temperature Energy Materials Research Center, Korea Institute of Science and Technology, Seoul 02792, Republic of Korea
[c] Ferrous Alloys Group, Korea Institute of Materials Science, Changwon 51508, Republic of Korea
[d] School of Materials Science and Engineering, Ulsan National Institute of Science and Technology, Ulsan 44919, Republic of Korea
[e] Department of Materials Engineering, Indian Institute of Science, Bangalore 560012, India

ARTICLE INFO

Article history:
Received 7 February 2017
Received in revised form 12 March 2017
Accepted 24 March 2017
Available online 31 March 2017

Keywords:
High-entropy alloy
Hydrogen embrittlement
Tensile test
Nanoindentation
Thermal desorption spectroscopy

ABSTRACT

The influence of hydrogen on the mechanical behavior of the CoCrFeMnNi high-entropy alloy (HEA) was examined through tensile and nanoindentation experiments on specimens hydrogenated via gaseous and electrochemical methods. Results show that the HEA's resistance to gaseous hydrogen embrittlement is better than that of two representative austenitic stainless steels, in spite of the fact that it absorbs a larger amount of hydrogen than the two steels. Reasons for this were discussed in terms of hydrogen-enhanced localized plasticity mechanism and the critical amount of hydrogen required for it. These were further substantiated by additional experiments on electrochemically charged specimens.

High-entropy alloys (HEAs) that comprise of three or more (nearly-) equiatomic metallic elements have attracted significant research attention since they were first introduced about a decade back [1,2] as they show exceptional mechanical properties, especially high strength-ductility combinations at both elevated and cryogenic temperatures [3–9]. However, HEAs' susceptibility to hydrogen embrittlement (HE) [10–14], if any, was not examined in detail. Future structural components made of HEAs are likely to be exposed to hydrogen (H) in the working environment of a number of potential applications. Some such examples are high-content H in the water reactor environment of nuclear power plants [15], H_2 gas in moist environments like ambient air in aerospace structures [16], and H stored either as liquid in cryogenic vessels for space shuttles [17,18] or as gas in high-pressure vessels for H transportation/storage [17]. Keeping this in view, it is essential to study the effect of H on the mechanical behavior of HEAs, which is the purpose of the work reported in this paper.

For this, we have selected CoCrFeMnNi HEA, which is one of the most widely investigated HEAs to date, as it crystallizes into a remarkably stable face-centered cubic (fcc) single phase [1,19]. It exhibits exceptional ductility and fracture toughness at cryogenic temperatures [6,20] and good resistance to creep [7]. HE of this alloy upon gaseous H charging was examined, since the sources of H that cause embrittlement are generally gaseous in nature, and compared with that of two austenitic stainless steels (SSs), 304 and 316L. Like HEA, these SSs also have fcc crystal structure. Moreover, the main constituent elements in all the three alloys are the same; they only differ in relative content in each alloy [5]. Importantly, since the effect of H on SSs has been extensively studied (e.g. Refs. [10,22–25].), well-documented data is readily available for comparison.

The CoCrFeMnNi HEA samples were prepared by vacuum induction casting of nominal mixtures of the corresponding metals with purity higher than 99 wt%. The cast ingot was hot-forged and then solution annealed at 1100 °C for 1 h to reach an equilibrium microstructural state. The annealed sample has a single fcc phase. The backscattered electron (BSE) image obtained by scanning electron microscopy (SEM; Nova NanoSEM 450, FEI Inc., Hillsboro, OR, USA) displayed in Fig. 1 shows homogeneous equiaxed grains with an average grain size of ~34 μm. For comparison purpose, solution-annealed 304 and 316L steels were also prepared. The nominal compositions of HEA and the two SSs are given in Table 1. All the HEA and SS specimens tested in this study (irrespective of H charging) were always ground initially with fine SiC papers (grit number up to 2000) and then with colloidal silica (0.05 μm) to a mirror finish, resulting in a final thickness of ~300 μm.

* Corresponding authors.
E-mail addresses: jinyoo@kist.re.kr (J.-Y. Suh), jijang@hanyang.ac.kr (J. Jang).

http://dx.doi.org/10.1016/j.scriptamat.2017.03.029
1359-6462/

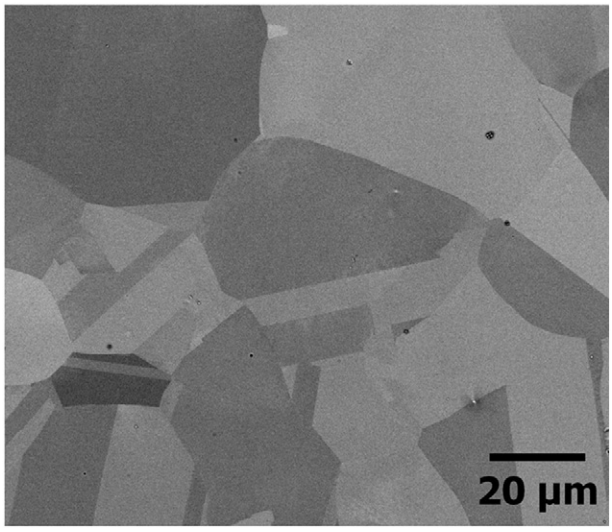

Fig. 1. SEM-BSE image showing the equiaxed grain structure with grain size ~34 μm of solution-annealed CoCrFeMnNi HEA.

Gaseous H charging (referred to as G-charging hereafter) of the HEA and two SS specimens was performed in a custom-made Sieverts apparatus at 300 °C under constant pressure of 15 MPa of gaseous H_2 for 72 h. In addition, electrochemical H charging (E-charging, hereafter) of the HEA was performed at RT using a potentiostat/galvanostat equipment (HA-151A, Hokuto Denko, Tokyo, Japan) in 1 N H_2SO_4 solution for 24 h under a constant current density of 100 mA/cm^2. To minimize the influence of outgassing, all the charged samples were immediately immersed always into liquid nitrogen and stored until further experiments, which were completed, in any case, within ~24 h after charging.

Flat dog-bone-shaped tensile samples with gauge length of 10 mm and gauge width of 1 mm were wire cut from the annealed bulk specimens. Tensile tests were carried out on these uncharged and G-charged subsize samples using a micro-tensile tester (MTest 300, Gatan Inc., Pleasanton, CA, USA) at a cross-head speed of 0.1 mm/min. Nanoindentation experiments were conducted using Nanoindenter-XP (formerly MTS; now Keysight Technologies, Santa Rosa, CA, USA) with two different three-sided pyramidal indenters (typical Berkovich and sharper cube-corner tips) at a peak load, P_{max}, of 100 mN under constant indentation strain rate $\dot{\varepsilon} = (dh/dt)/h = 0.025\ s^{-1}$ where h is indentation depth and t is the time. Fractography on the tensile tested samples and imaging of the indentation impressions was performed by SEM. The indentation impressions were additionally profiled with an atomic force spectroscope (AFM; XE-100, Park Systems, Suwon, Korea). For the quantitative analysis of the H content in the charged samples, thermal desorption spectroscopy (TDS) was performed with a quadrupole mass spectroscope (EX0014, R-DEC Company, Tsukuba, Japan) at a constant heating rate of 5 °C/min to a maximum temperature of ~800 °C.

Representative engineering stress vs. engineering strain responses of the G-charged HEA, 304 and 316L SSs, as well as their uncharged counterparts are displayed in Fig. 2. As expected, the ductility of both the SSs gets reduced markedly upon charging. Such embrittlement was absent in HEA, with the relative loss in ductility due to H charging being merely ~5%. For comparison, it is ~61% and ~27% for 304 and 316L SSs respectively. It appears that G-charging also does not affect the yield strength, flow stresses, or strain hardening rate of HEA in any significant manner. Fig. 2b and c show both low- and high-magnification fractographs of the tensile tested specimens of HEA in uncharged and charged conditions, respectively. Both the fracture surface morphologies are similar, and consist of dimples, indicating ductile fracture. This observation further supports HEA's resistance to H-induced embrittlement.

Table 1
Nominal chemical compositions (wt%) of CoCrFeMnNi HEA (transferred from nominal 20 at.% for each element), 304, and 316 SSs.

	Co	Cr	Fe	Mn	Ni	C	Si	Mo	V	N	Cu
HEA	21.0	18.6	19.9	19.6	20.9						
304	0.01	17.74	Bal.	1.05	7.83	0.05	0.56	0.20	0.01	0.006	
316L	0.19	16.50	Bal.	1.29	9.77	0.02	0.50	2.07	0.10	0.02	0.27

'Is the superior embrittlement resistance of HEA due, possibly, to the H content in it being lower than those of the two steels?' To answer this question, the quantity of H in the G-charged HEA, 304, and 316L samples was measured by TDS, whose results are displayed in Fig. 3. In all the three cases, the peak desorption occurs at similar temperatures. This, in turn, indicates that the sites within the fcc lattice, which H occupies, may be similar in all the three alloys. They correspond to interstitial lattice sites and weak H trapping defects such as dislocations [26,27]. Importantly, Fig. 3 shows that the desorbed H content from HEA (~76.5 ppm) is higher than that from either of the SSs. It also is higher than most literature values of SSs exposed to higher H_2 pressure than that in the present study [28–30]. Since no new phase was found through X-ray diffraction analysis after H charging of the HEA [21], such high H solubility may be attributed to the relatively high content of Cr and Mn in HEA compared to in other austenitic SSs, since the two elements were found to be crucial in influencing H solubility [22,31]. In addition, the lattice distortion in HEA can also be one of the contributing factors for the enhanced solubility as demonstrated for the solid state H storage application of HEA [32]. On this basis, we conclude that the absence of HE in HEA is not due to lack of H and seek an alternative explanation for it.

Two widely-accepted micromechanisms for HE in SSs are the following: (a) stress-induced austenite-to-martensite transformation [24,28] and (b) H-enhanced localized plasticity (HELP) [11,33,34]. Since stress-induced transformation was not observed to occur in the CoCrFeMnNi HEA [6,19,20], the former mechanism can be excluded. In HELP, the dissolved H enhances local dislocation mobility and slip planarity [25,33], which in turn promotes cleavage fracture. Therefore, HE through HELP is more pronounced in materials that are already prone to planar slip [33,34]. Systematic transmission electron microscopy by George and coworkers [20,35] do indeed show that the CoCrFeMnNi HEA deforms primarily through planar slip. Therefore, it is natural to anticipate that the HELP mechanism will be of significance in this HEA. But planar slip is only a necessary condition for HELP. For it to occur, sufficiently high and local H content is also essential [36,37]. This is especially important when H diffusivity is sluggish, which is the case in for fcc metals and alloys [26]. In contrast, and for example, fast diffusion of H to highly-stressed regions in body-centered cubic (bcc) metals amplifies the effect of H on the plastic deformation in them. That high local H content is necessary for HELP in fcc metals is further supported by the observation that SSs such as 310 and some 316 steels with high Ni equivalent, which also do not undergo strain-induced martensitic transformation, are not prone to HE in H_2 gas atmosphere [22,29,34,38], but are usually susceptible to HE upon E-charging [23,36,37]. This is because cross-slip dominates plasticity in such SSs and thus HE can occur if and only if the H content in the SS upon charging is extremely high, which is possible in E-charging [30,39].

From the above discussion, it is reasonable to conclude that the G-charged CoCrFeMnNi HEA did not get embrittled possibly because the local H content upon charging is below the threshold level required for triggering HELP. To elaborate this further through experiments, the HEA was exposed to a much harsher H environment through the E-charging process. Subsequently, nanoindentation was utilized to evaluate and compare the mechanical responses of uncharged, G-charged, and E-charged samples. Representative nanoindentation load–displacement (P-h) curves, obtained by using both Berkovich and cube-corner indenters, are provided in Fig. 4a. The hardness values, which were

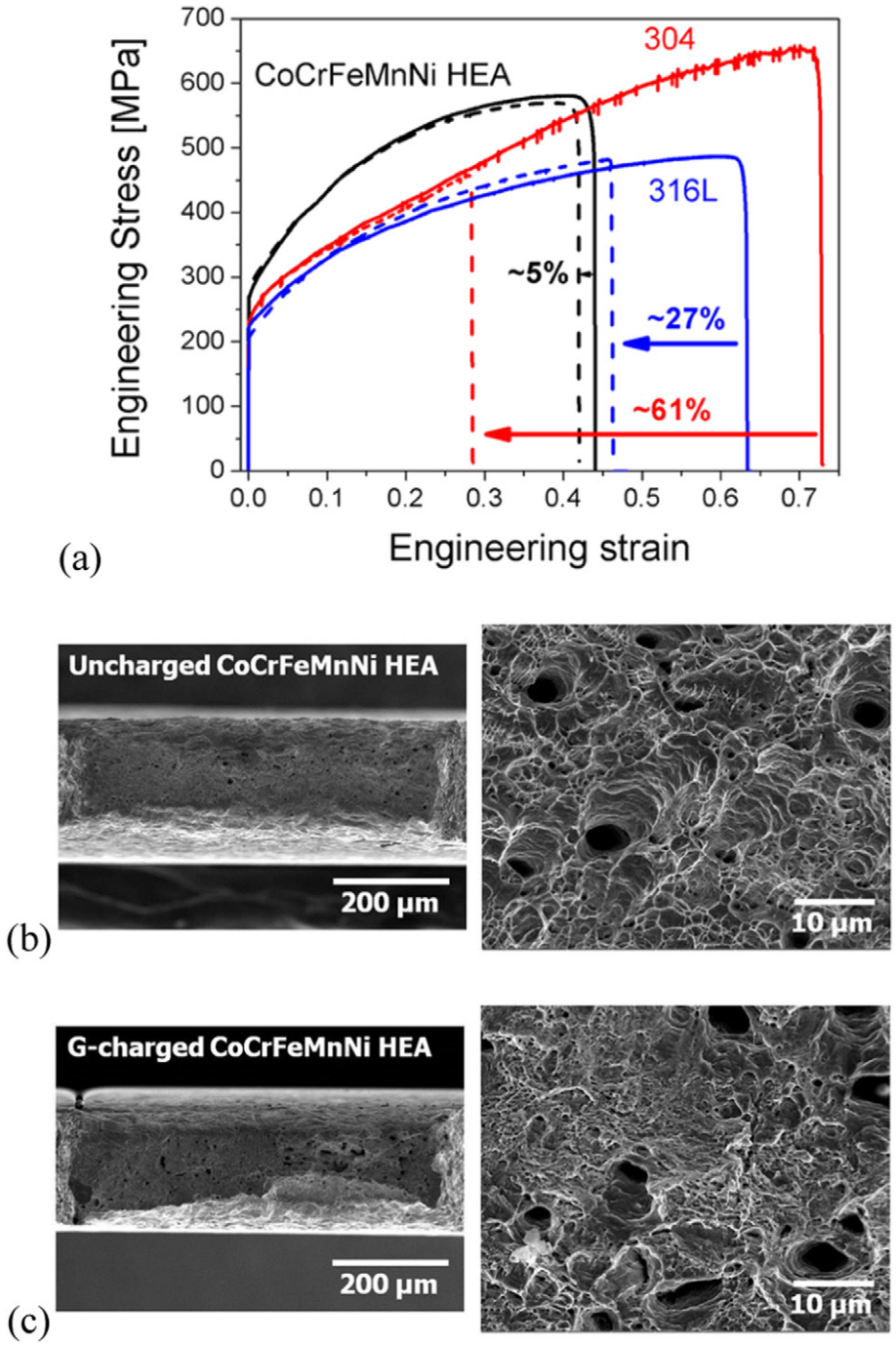

Fig. 2. Results from tensile tests. (a) Engineering stress–engineering strain curves (with the numbers showing ductility loss, el_{loss}, due to G-charging). The low- and high-magnification SEM images shows the fracture surfaces of (b) uncharged and (c) G-charged HEA.

estimated from them by the Oliver-Pharr method [40], are summarized in Table 2. In agreement with the tensile test results, no significant change in the hardness is noted upon G-charging. In contrast, substantial enhancement in the hardness (by ~63% in Berkovich and ~37% in cube corner) occurs upon E-charging.

Observations of the surface morphology around the cube-corner nanoindentations, displayed in Fig. 4b, provide further support to the H effects on the indentation-induced plasticity. Cube-corner indenter, being sharper, induces higher stresses and strains underneath the indenter. This, in turn, leads to pronounced impression morphologies [41,42]. The morphologies around the indents in the uncharged and G-charged specimens appear similar, with a large number of slip-traces. These not only confirm the planar nature of slip in the HEA examined, but also affirm the earlier observation that G-charging does not affect the plasticity in the HEA in any significant manner. In contrast, the number of slip steps around the indents made on the E-charged sample is far smaller, confirming a significantly reduced plasticity upon E-charging. A comparison of the AFM profiles, displayed in Fig. 4b, indicates that both the height and spacing of the slip steps around nanoindentations in the E-charged sample are larger than those in the uncharged one. This observation further supports the notion of reduced cross-slip and thus more enhanced slip planarity in the former [25]. These observations provide evidence for the reduced plastic deformation susceptibility and enhanced slip planarity by E-charging vis-à-vis G-charging.

At this juncture, it is interesting to note that the overall H content in the E-charged CoCrFeMnNi HEA specimen, which we have reported in a

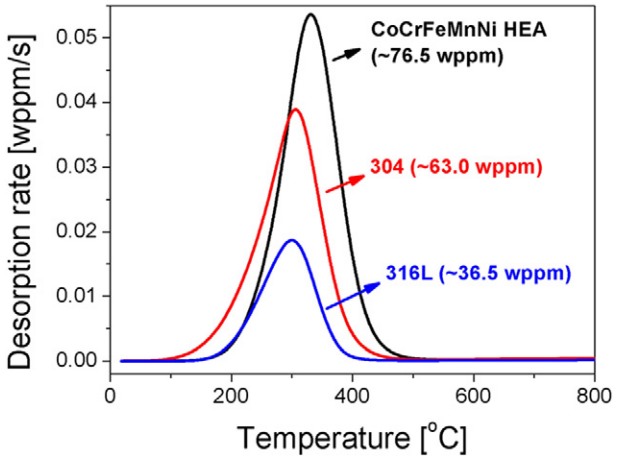

Fig. 3. H desorption curves obtained from TDS measurements of CoCrFeMnNi HEA, 304 SS, and 316L SS samples that were G-charged under the exactly same condition.

recent study [21], is ~45.0 wppm, i.e., less than that in the G-charged specimen of the present study. Then, the homogeneity of H concentrations in both cases comes into focus. In the G-charged sample, it is reasonable to expect a homogeneous distribution through the thickness of the sample since the time (72 h) - temperature (300 °C) combination of charging is sufficient for H diffusion throughout the specimen [37,43]. In contrast, E-charging was carried out at room temperature (RT), where the hydrogen diffusivity is much lower, and for a shorter duration (24 h). Note that the temperature dependence of hydrogen diffusivity is significant for fcc metals due to the large activation barrier energy for diffusion. Therefore, a steep gradient in the H concentration in the E-charged sample is possible. It, as a function of the distance from the surface, x, can be estimated by [43]:

$$C(x, t_c) = C_0\left[1 - erf\left(\frac{x}{2\sqrt{D_H t_c}}\right)\right], \quad (1)$$

where t_c is the charging time, and D_H is H diffusivity in HEA. Given the similarity in the composition and the crystal structure, D_H is assumed to be the same as that of 300-series SS (~3.17×10^{-16} m^2/s at RT [31]). The concentration profiles of H in the samples, estimated using Eq. (1), are shown in Fig. 4c for both G- and E-charged samples. We see from it that H is mostly concentrated near the surface in the latter (see [21,44] for details). At the surface, C is as high as ~1143 wppm, which can conceivably trigger HELP. Since nanoindentation probes the surface properties, a marked increase hardness values of the E-charged HEA specimen was observed [21,25,45].

In summary, the influence of gaseous and electrochemical H charging on the mechanical behavior of the CoCrFeMnNi HEA was investigated through tensile and nanoindentation experiments. The results show that G-charged HEA, in spite of its strong ability to absorb H, is resistant to embrittlement whereas marked ductility losses were noted for 304 and 316L SSs subjected to identical charging conditions. Through nanoindentation experiments on both G- and E-charged specimens, we reason that the former fails to embrittle HEA because the H content upon charging is below the threshold required for triggering the H-enhanced localized plasticity mechanism.

The work at Hanyang University was supported by the National Research Foundation of Korea (NRF) grants funded by the Ministry of Science, ICT & Future Planning (MSIP) (No. 2014M2A8A1030385 and No. 2015R1A5A1037627). The work at KIST was supported by the Convergence Agenda Program (CAP) of the Korea Research Council of Fundamental Science and Technology. The authors wish to thank Mr. Han-Jin Kim (KIST) and Mr. Chang-Geun Lee (KIMS) for their valuable supports with experiments.

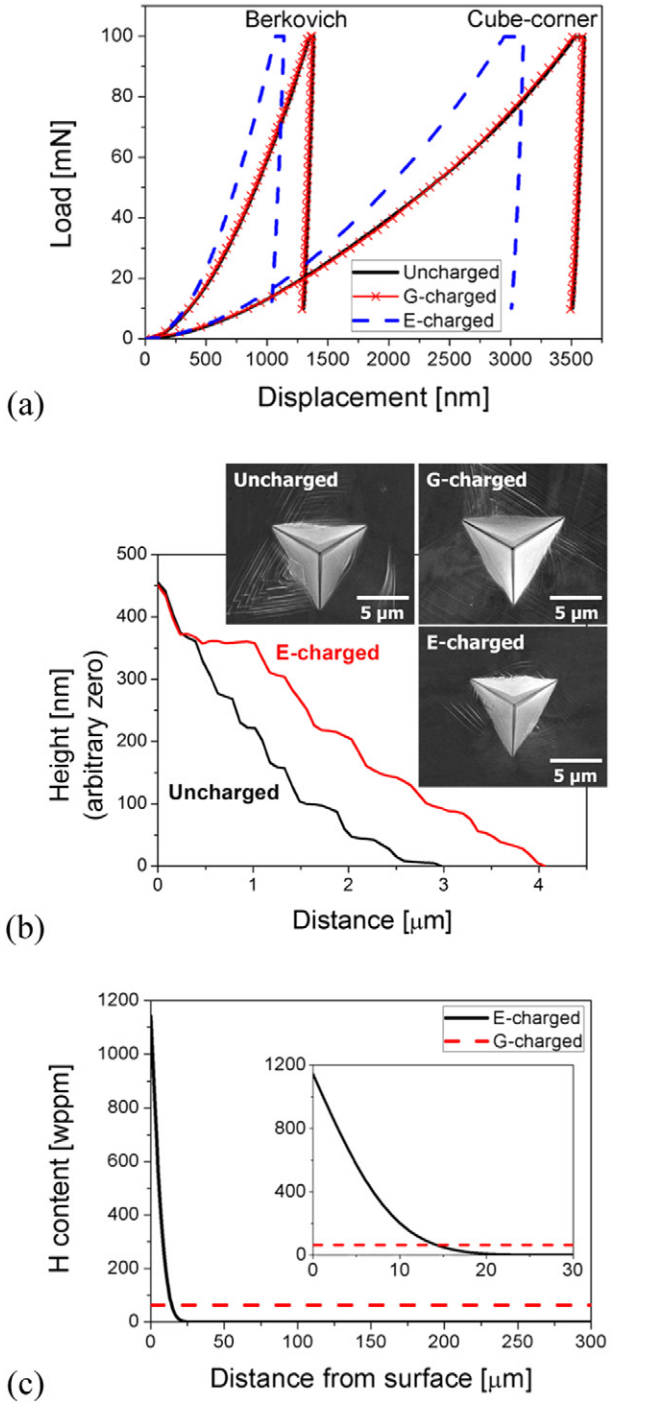

Fig. 4. G-charging vs. E-charging of CoCrFeMnNi HEA. (a) Representative load-displacement curves of uncharged, G-charged, and E-charged specimens by nanoindentation tests with Berkovich and cube-corner indenters. (b) Representative SEM images of cube-corner indentation impressions with AFM profiles showing the slip steps for uncharged and E-charged specimens. (c) Estimated H content distributions along specimen thickness of G- and E-charged HEAs with the inset showing an enlarged view of the curves within 30 μm near surface.

Table 2
Hardness values of uncharged, G-charged, and E-charged CoCrFeMnNi HEAs estimated from nanoindentation tests with Berkovich and cube-corner indenters.

Condition of HEA	Nanoindentation hardness (GPa)	
	Berkovich	Cube-corner
Uncharged	2.69 ± 0.06	2.55 ± 0.10
G-charged	2.74 ± 0.09	2.54 ± 0.07
E-charged	4.39 ± 0.20	3.49 ± 0.06

References

[1] B. Cantor, I.T.H. Chang, P. Knight, A. Vincent, Mater. Sci. Eng. A 375–377 (2004) 213–218.
[2] J.-W. Yeh, S.-K. Chen, S.-J. Lin, J.-Y. Gan, T.-S. Chin, T.-T. Shun, C.-H. Tsau, S.-Y. Chang, Adv. Eng. Mater. 6 (2004) 299–303.
[3] Y. Zhang, T.T. Zuo, Z. Tang, M.C. Gao, K.A. Dahmen, P.K. Liaw, Z.P. Lu, Prog. Mater. Sci. 61 (2014) 1–93.
[4] Y.F. Ye, Q. Wang, J. Lu, C.T. Liu, Y. Yang, Mater. Today 19 (2016) 349–362.
[5] D.B. Miracle, O.N. Senkov, Acta Mater. 122 (2017) 448–511.
[6] B. Gludovatz, A. Hohenwarter, D. Catoor, E.H. Chang, E.P. George, R.O. Ritchie, Science 345 (2014) 1153–1158.
[7] D.-H. Lee, M.-Y. Seok, Y. Zhao, I.-C. Choi, J. He, Z. Lu, J.-Y. Suh, U. Ramamurty, M. Kawasaki, T.G. Langdon, J.-i. Jang, Acta Mater. 109 (2016) 314–322.
[8] V. Ocelik, N. Janssen, S.N. Smith, J.Th.M. De Hosson, JOM 68 (2016) 1810–1818.
[9] J.C. Rao, V. Ocelik, D. Vainchtein, Z. Tang, P.K. Liaw, J.Th.M. De Hosson, Mater. Lett. 176 (2016) 29–32.
[10] M.R. Louthan, G.R. Caskey, J.A. Donovan, D.E. Rawl, Mater. Sci. Eng. 10 (1972) 357–368.
[11] H.K. Birnbaum, P. Sofronis, Mater. Sci. Eng. 176 (1994) 191–202.
[12] I.M. Robertson, P. Sofronis, A. Nagao, M.L. Martin, S. Wang, D.W. Gross, K.E. Nygren, Metall. Mater. Trans. A 26 (2015) 2323–2341.
[13] A. Barnoush, H. Vehoff, Acta Mater. 58 (2010) 5274–5285.
[14] Y. Zhao, I.-C. Choi, M.-Y. Seok, M.-H. Kim, D.-H. Kim, U. Ramamurty, J.-Y. Suh, J.-i. Jang, Acta Mater. 78 (2014) 213–221.
[15] R.S. Dutta, J. Nucl. Mater. 393 (2009) 343–349.
[16] G. Hénaff, G. Odemer, A. Tonneau-Morel, Int. J. Fatigue 29 (2007) 1927–1940.
[17] H. Barthélémy, Int. J. Hydrog. Energy 37 (2012) 17364–17372.
[18] R.R. Boyer, Mater. Sci. Eng. A 213 (1996) 103–114.
[19] F. Otto, N.L. Hanold, E.P. George, Intermetallics 54 (2014) 39–48.
[20] F. Otto, A. Dlouhý, Ch. Somsen, H. Bei, G. Eggeler, E.P. George, Acta Mater. 61 (2013) 5743–5755.
[21] Y. Zhao, D.-H. Lee, J.-A. Lee, W.-J. Kim, H.N. Han, U. Ramamurty, J.-A. Suh, J.-i. Jang, Int. J. Hydrog. Energy (2017) http://dx.doi.org/10.1016/j.ijhydene.2017.02.061.
[22] G.R. Caskey, in: R.A. Oriani, J.P. Hirth, M. Smialowski (Eds.), Hydrogen Degradation of Ferrous Alloys, Noyes Publications, Park Ridge, NJ 1985, pp. 822–862.
[23] M.B. Whiteman, A.R. Troiano, Corrosion 21 (1965) 53–56.
[24] G. Han, J. He, S. Fukuyama, K. Yokogawa, Acta Mater. 46 (1998) 4559–4570.
[25] K.A. Nibur, D.F. Bahr, B.P. Somerday, Acta Mater. 54 (2006) 2677–2684.
[26] A. Turnbull, in: R.P. Gangloff, B.P. Somerday (Eds.), Gaseous Hydrogen Embrittlement of Materials in Energy Technologies, Woodhead Publishing Ltd., Cambridge 2012, pp. 89–128.
[27] J.H. Ryu, Y.S. Chun, C.S. Lee, H.K.D.H. Bhadeshia, D.W. Suh, Acta Mater. 60 (2012) 4085–4092.
[28] L. Zhang, Z. Li, J. Zheng, Y. Zhao, P. Xu, C. Zhao, X. Li, Int. J. Hydrog. Energy 38 (2013) 8208–8214.
[29] C. San Marchi, T. Michler, K.A. Nibur, B.P. Somerday, Int. J. Hydrog. Energy 35 (2010) 9736–9745.
[30] A.-M. Brass, J. Chêne, Corros. Sci. 48 (2006) 3222–3242.
[31] C. San Marchi, B.P. Somerday, S.L. Robinson, Int. J. Hydrog. Energy 32 (2007) 100–116.
[32] M. Sahlberg, D. Karlsson, C. Zlotea, U. Jansson, Sci. Rep. 6 (2016) 36770.
[33] C. San Marchi, B.P. Somerday, X. Tang, G.H. Schiroky, Int. J. Hydrog. Energy 33 (2008) 889–904.
[34] T. Michler, C. San Marchi, J. Naumann, S. Weber, M. Martin, Int. J. Hydrog. Energy 37 (2012) 16231–16246.
[35] G. Laplanche, A. Lostka, O.M. Horst, G. Eggeler, E.P. George, Acta Mater. 118 (2016) 152–163.
[36] D.G. Ulmer, C.J. Altstetter, Acta Metall. Mater. 39 (1991) 1237–1248.
[37] D.P. Abraham, C.J. Altstetter, Metall. Mater. Trans. A 26 (1995) 2849–2858.
[38] L. Zhang, M. Wen, M. Imade, S. Fukuyama, K. Yokogawa, Acta Mater. 56 (2008) 3414–3421.
[39] Y. Zhao, M.-Y. Seok, I.-C. Choi, Y.-H. Lee, S.-J. Park, U. Ramamurty, J.-Y. Suh, J.-i. Jang, Scr. Mater. 107 (2015) 46–49.
[40] W.C. Oliver, G.M. Pharr, J. Mater. Res. 7 (1992) 1564–1583.
[41] Y. Zhao, I.-C. Choi, M.-Y. Seok, U. Ramamurty, J.-Y. Suh, J.-i. Jang, Scr. Mater. 93 (2014) 56–59.
[42] J.-i. Jang, G.M. Pharr, Acta Mater. 56 (2008) 4458–4469.
[43] J. Crank, The Mathematics of Diffusion, second ed. Oxford University Press, London, 1975.
[44] A.E. Pontini, J.D. Hermida, Scr. Mater. 37 (1997) 1831–1837.
[45] K.R. Morasch, D.F. Bahr, Scr. Mater. 45 (2001) 839–845.